Effects of Highly Cystalline and Conductive Polyaniline/Graphene Oxide Composites on the Corrosion Protection Performance of a Zinc-Rich Epoxy Coating

B. Ramezanzadeh, M.H. Mohamadzadeh Moghadam, N. Shohani, M. Mahdavian

PII: S1385-8947(17)30417-5
DOI: http://dx.doi.org/10.1016/j.cej.2017.03.061
Reference: CEJ 16657

To appear in: *Chemical Engineering Journal*

Received Date: 30 November 2016
Revised Date: 14 February 2017
Accepted Date: 14 March 2017

Please cite this article as: B. Ramezanzadeh, M.H. Mohamadzadeh Moghadam, N. Shohani, M. Mahdavian, Effects of Highly Cystalline and Conductive Polyaniline/Graphene Oxide Composites on the Corrosion Protection Performance of a Zinc-Rich Epoxy Coating, *Chemical Engineering Journal* (2017), doi: http://dx.doi.org/10.1016/j.cej.2017.03.061

Effects of Highly Cystalline and Conductive Polyaniline/Graphene Oxide Composites on the Corrosion Protection Performance of a Zinc-Rich Epoxy Coating

B.Ramezanzadeh*[a], M. H. Mohamadzadeh Moghadam[b], N.Shohani[a], M.Mahdavian[a]

a. Surface Coating and Corrosion Department, Institute for Color Science and Technology, Tehran, Iran.

b. Condensed Matter National Laboratory, Institute for Research in Fundamental Sciences, 19395-5531, Tehran, Iran.

Ave, P.O. Box: 15875-4413, Tehran, Iran

**Corresponding author: E-mail: ramezanzadeh@aut.ac.ir; Fax: +98 2122947537; Tel: +98 2122969771*

Abstract: This study reports a new strategy for providing ZRC with enhanced cathodic and barrier protection mechanisms simultaneously. For this purpose, the graphene oxide (GO) nanosheets were modified by highly crystalline and conductive polyaniline (PANI) nanofibers in the form of Emeraldine salt (ES) through an in situ polymerization of aniline in the presence of GO as an oxidant. The aniline polymerization in the presence of GO and the PANI nanofibers deposition on the GO surface were exhibited by Fourier transform infrared (FT-IR) spectroscopy and high resolution-transmittance electron microscopy (HR-TEM). In addition to these the X-ray diffraction (XRD) patterns confirmed the deposition of highly crystalline PANI nanofibers on the GO and between the GO layers. Inclusion of 0.1 wt.% GO and GO-PANI nanosheets into the ZRC sample remarkably enhanced its corrosion protection performance. Salt spray, open circuit potential (OCP) and electrochemical impedance spectroscopy (EIS) measurements revealed that both the cathodic protection properties and barrier performance of the ZRC were improved after addition of 0.1 wt.% GO and GO-PANI nanossheets to the ZRC sample. The most pronounced improvement in the ZRC properties was obtained using GO-PANI. The results obtained from field-emission scanning electron microscopy (FE-SEM), energy dispersive spectroscopy and XRD analysis confirmed lower

degree of zinc particles oxidation and steel substrate corrosion in the case of ZRC including GO-PANI nanosheets compared to other samples.

Keywords: Highly cystalline and conductive polyaniline/graphene oxide; Epoxy zinc-rich; Corrosion protection; FT-IR; HR-TEM; EIS

1. Introduction

Several coating systems have been used to control or mitigate the corrosion processes that take place on the steel surface in exposure with severe environments including organic, inorganic, and hybrid protective coatings [1-3]. Among these methods application of organic coatings is the most popular and effective strategy to protect the steel structures against corrosion [4, 5]. Depending on the chemical formulation and the type and amount of the ingredients of the organic coatings they can protect the steel from corrosion through three main mechanisms; (a) barrier, (b) sacrificial and (c) inhibiting features [6-11].Organic coatings can provide a physical barrier against diffusion of corrosive agents such as H_2O, O_2 and ions i.e. Cl^- to the steel surface. However, they cannot show protective performance in the case of a slight mechanical damage creation on the coating. Zinc-rich coatings, i.e epoxy zinc-rich, are another type of organic coatings that can protect the metals against corrosion for long exposure times in severe environments, even when there is mechanical damage. Addition of high amount of zinc particles to the epoxy resin provides a coating system with cathodic protection properties [12-13]. In this case the continuous electrical contact between the zinc metal particles and steel substrate provides a galvanic cell, where the steel substrate acts as cathode and zinc particles behave as sacrificial anodes. For a common zinc-rich coating with proper sacrificial properties the ratio of pigment volume concentration (PVC)/critical pigment volume concentration (CPVC) is >1 [12-17]. The dominant protection mechanism of zinc rich coating at earlier stages of its service life is cathodic protection but as

the time passes the electrical contact between the zinc particles and steel substrate rapidly decreases as a result of fast oxidation of zinc particles. The zinc oxide corrosion products creation in the coating matrix results in the decrease of coating porosity and decrease in the coating sacrificial properties through reducing the amount of electrolyte that reaches the steel surface. In this case, at longer exposure times, the coating protection mechanism is a combination of barrier and sacrificial properties [16-20]. So the presence of high amount of zinc particles in the zinc-rich coating cannot guarantee its cathodic protection for a long time in severe environments. Inclusion of high amount of zinc particles increases the coating porosity and therefore corrosive agents easily diffuse into the coating, leading to the rapid loss of the electrical connection among zinc particles and with the carbon steel surface.

Attempts have been performed to enhance the cathodic protection duration of zinc-rich coating through inclusion of different types of fillers and additives. The effect of addition of zinc nanoparticles to the zinc-rich coating on its cathodic protection performance has been studied by Schaefer et al. [21]. In a work done by Arianpouya et al. [22] the effect of addition of a mixture of nanozinc and nanoclay on the zinc-rich coating protection performance was reported. They revealed that inclusion of a small quantity of nanozinc and nanoclay particles could remarkably enhance the coating performance through improving both sacrificial and barrier properties of the zinc-rich coating, simultaneously. Jagtap et al. [23] reported significant improvement of the barrier properties and service life of zinc-rich coating after addition of small amounts of zinc oxide particles. In another study Zhang et al. [24] reported the beneficial role of addition of the modified silicon-based vehicle and lamellar Zn (Al) pigments on the zinc rich coating protective properties. The effect of nano-size alumina modified by polypyrrole on the zinc-rich coating corrosion resistance enhancement has been reported by Gergely et al. [25]. In our previous studies the effects of addition of lamellar aluminum and iron oxide pigments [13] and surface modified aluminium nanoparticles [26]

on the corrosion protection performance of the epoxy zinc-rich coating have been evaluated. In other studies carbon nanotube [27], polyaniline clay (PAniC) nanocomposites [28], nanoclay [29], propargyl alcohol impregnated mesoporous titanium dioxide [30] and zinc powders [31] modified with organosilanes were added to the zinc-rich coating to enhance its protection performance. In all of these studies the improvement of corrosion protection performance of zinc-rich coating has been reported.

An attractive option for improving the zinc rich coating corrosion performance is inclusion of an advanced nanomaterial based on graphene oxide. GO is a single-atom-thick sheet of hexagonally arrayed sp^2-bonded carbon atoms with many functional groups i.e. hydroxyl, carbonyl, carboxyl and epoxy groups [32-36]. These are reactive sites for covalent and/or non-covalent functionalization with organic and/or inorganic compounds, leading to the improvement of the interfacial interactions between the graphene oxide nanosheets and polymers [35-41]. It has been demonstrated in recent studies that inclusion of functionalized GO nanosheets into the polymeric coatings remarkably enhances their corrosion protection performance. GO sheets are impermeable against water, oxygen and ions diffusion and provide a good barrier as a result of theirs high surface area [42-62]. So this nanomaterial would be a good candidate for enhancing the protection performance of a zinc-rich coating. In addition, covalent functionalization of GO can be done by conducting polymers (CPs) which have received a considerable attention in recent years because of their unique electrochemical properties. It has been shown that CPs can effectively protect the metals from corrosion through passivation mechanism [63-64]. Armelin et al. [65] and Akbarinezhad et al. [28] have shown the beneficial role of PANIs on the corrosion protection performance improvement of the zinc-rich coating. However to the best of our knowledge there is no report on using GO and GO-PANI nanosheets on the corrosion protection performance of zinc rich coating.

In this study the influence of GO and GO-PANI nanosheets on the corrosion protection performance of a zinc rich coating has been studied. First the GO was synthesized using expendable graphite powder and then it was converted to graphene oxide by a Modified Hummers' method. In the next step, the highly crystalline and conductive PANI nanofibers were deposited on the GO surface through an in situ polymerization of aniline in the presence of GO as an oxidant. After characterization of GO and GO-PANI by FT-IR, XRD and HR-TEM analyses, 0.1 wt.% GO and GO-PANI nanosheets were separately incorporated into the ZRC. Finally, the corrosion protection performance of the ZRC, GO/ZRC and GO-PANI/ZRC samples were examined by OCP, EIS and salt spray tests.

.

2. Experimental

2.1. Raw materials

The zinc dust with average particle size, oil absorption and density of 5 μm, 6.7 g 100 g^{-1}pigment, 6.95 g cm^{-3}, respectively was prepared from Iran Zinc Powder Co. Graphene oxide nanosheets were obtained through a modified Hummer's method from an expandable graphite powder, Kropfmuehl Graphite Co. Germany. The expansion rate and grain size of the graphite used were 350-700 cm^3/g and 80%>300 μm, respectively. Sulfuric acid (Merck 98%, pure), zinc nitrate (Merck), sodium nitrite (Merck), potassium permanganate (Merck), hydrogen peroxide (Merck) and dimethylformamide (DMF, Merck Co.) were used without further purification. The steel panels with dimension of 10 cm ×8 cm ×0.2 cm and chemical composition (wt.%) of: 0.05% S, 0.5% Mn, 0.12% C, 0.3% Si, 0.045% P and balanced Fe) were prepared from Foolad Mobarakeh Co (Iran). Epon 828 as a solvent free epoxy resin and Epikure F205 as a polyamine hardener were purchased from Shell, USA and Kian Co., Iran, respectively.

2.2. GO and GO-PANI synthesis procedures

GO nanosheets were synthesized through modified Hummer's method [66] from expandable graphite (EG). In the first step 1 g of EG was added to 120 mL concentrated sulfuric acid and stirred for 2 h. In the next step, 6 g of $KMnO_4$ and 1 g of $NaNO_3$ were gradually added to the solution and mixed for 72 h. Finally, the mixture was diluted by 600 mL deionized water and then 3-5 ml of H_2O_2 (35%) was added to the mixture for ending the oxidation reaction. The graphite oxide obtained was washed and centrifuged for 2 min at 4000 rpm with a mixture of 1M HCl solution and DI water, and this procedure repeated three times separately.

GO-PANI was synthesized by a novel approach proposed by Mohamadzadeh Moghadam et al. [63]. In this method 1 mL of aniline monomer was added to 10 cc of 1 M HCl solution and stirred for 10 min to reach a homogenous solution. Then, 0.2 g of GO was dispersed in DI water and added to the previous solution under nitrogen purging. The mixture was stirred at room temperature for one week. Finally, the products obtained were centrifuged and washed to remove the impurities and unreacted materials. The synthesis procedures are schematically presented in **Figure 1.**

Figure 1

2.3. ZRC, GO/ZRC and GO-PANI/ZRC composites preparation and application

For a common type of zinc rich coating the ratio of pigment volume concentration (PVC)/critical pigment volume concentration (CPVC) should be >1 to provide proper cathodic protection. So, before inclusion of zinc dust into the epoxy coating the CPVC was calculated according to Eq.1.

$$\mathrm{CPVC} = 1 + \frac{1}{1 + \frac{O \times D}{93.2}} \quad (1)$$

where O and D are the oil absorption and density of the zinc dust, respectively. In this study the PVC and PVC/CPVC of the ZRC sample were 59.36 and 1.05, respectively. To prepare

GO/ZRC and GO-PANI/ZRC samples 10 cc DMF solutions containing 0.1 g GO and GO-PANI were separately added to the epoxy resin and the mixture was sonicated for two min. Then, the zinc dust (PVC=59.36) was added to the epoxy resin and mixed with a mixer at 1000 rpm. Finally, the polyamine curing agent was mixed with ZRC, GO/ZRC and GO-PANI/ZRC composites with ratio of 1:2 w/w. The ZRC, GO/ZRC and GO-PANI/ZRC samples were applied on the steel sheets that were abraded by sand papers of 600, 800 and 1200 grades followed by acetone rinsing. The coated samples were kept at room temperature for 15 days for completion of curing. The coating thickness after curing was about 70±5 μm.

2.4. Characterization

2.4.1. GO and GO-PANI characterization

Fourier Transform Infrared (FT-IR) spectroscopy (Perkin Elmer, USA) was employed to investigate the chemical structure of GO and GO-PANI nanosheets. The test was performed on KBr pellet within wavenumber range of 400-4000 cm^{-1}. The phase composition of GO and GO-PANI nanosheets was examined by XRD analysis (Philips X-ray spectrometer, PW 1800 type, Netherlands) with Cu-ka filament and X-ray wavelength of 1.5406 Å. The PANI nanofibers deposition on the GO sheets was evaluated by a HR-TEM (Tecnai G2 F20S-TWIN 200KV) technique. The electrical conductivity of PANI and GO-PANI was recorded by a lab-made two-point probe apparatus. Disk-shaped samples were prepared by pressing an appropriate amount of materials at 4000 psi. The radius of disk and thickness of the disk were 1 cm and 0.5 mm, respectively. The electrical resistivity was measured for three times for each sample. Finally, electrical conductivity was calculated according to the formula [80]:

$$\sigma = \frac{1}{\rho} = \frac{l}{AR} \qquad (2)$$

in which σ, ρ, l, A, and R are electrical conductivity ($S.m^{-1}$), electrical resistivity (ohm.m), disk thickness (m), and disk surface area (m^2) respectively. Differential scanning calorimetry

(DSC, TA instrument) was performed from room temperature (25 °C) to 290 °C with a ramp of 10 °C/min under nitrogen atmosphere.

2.4.2. Corrosion studies

The cathodic protection properties of the ZRC, GO/ZRC and GO-PANI/ZRC samples were tested through OCP measurements (vs SCE) at different period of times. The corrosion protection performance of the samples was studied by salt spray test. This test was performed in a salt spray cabin S85 V400 (made by Pars Horm Co.) according to ASTM B117. In this test, a 5 wt.% NaCl solution (45 °C) was continually sprayed on the samples with X-cut scribes. Electrochemical impedance spectroscopy (Iviuom Compactstat) was employed to investigate the corrosion protection performance of the steel sheets coated with ZRC, GO/ZRC and GO-PANI/ZRC. This test was carried out on 1 cm^2 of each sample in 3.5 wt.% NaCl solution through a conventional electrochemical cell including Platinum as counter, Ag/AgCl as reference and coated steel panel as working electrodes, respectively. The test was done at OCP in the frequency range and amplitude sinusoidal voltage of 10 kHz to 10 mHz (peak to zero) and 10 mV, respectively.

2.4.3. Surface analysis

The surface morphology of the ZRC, GO/ZRC and GO-PANI/ZRC samples was evaluated by FE-SEM model MIRA TESCAN before and after 1000 h exposure to salt spray test. Also, the phase composition of these samples was studied by XRD analysis (Philips X-ray spectrometer, PW 1800 type, Netherlands) after 1000 h salt spray exposure. The EDS spectra were obtained from the surface of various samples before and after 30 days immersion in 3.5 wt.% NaCl solution. Pull-off test was performed on the ZRC, GO/ZRC and GO-PANI/ZRC samples after 200 h salt spray test to investigate the coatings adhesion properties. The test was done by a Posi test pull-off adhesion tester (DEFELSKO).

3. Results and discussion

3.1. GO and GO-PANI characterization

The chemical structures of GO and GO-PANI nanosheets were characterized by FT-IR analysis. According to **Figure 2a** there are characteristic peaks of GO at 1725 and 1415 cm^{-1} which correspond to the stretching of C=O and C-O bonds of COOH groups [67], respectively. The stretching of C-O bond related to the epoxide groups, the stretching of aromatic C=C, the intensive and broad peak O-H of carboxylic groups and the absorption of C-H stretching can be seen at 1260, 1625, 3435 and 2950 cm^{-1}, respectively. These all conform that the GO was successfully synthesized and the epoxy, hydroxyl and carboxylic groups are present on the GO nanosheets that are in accordance with the results reported in the literature. According to the FT-IR spectrum of GO-PANI the characteristic peaks of both PANI and GO can be observed. The main characteristic peaks related to PANI structure can be seen at 1559, 1480 and 1300 cm^{-1} which correspond to the C=C stretching of benzenoid ring, C=N stretching of quinoid ring and C-N stretching, respectively [68-73]. The bands appeared in the wavenumber range of 650 to 850 cm^{-1} are attributed to the bending deformation C-H out of plane and the band at 484, 521, and 600 cm^{-1} are corresponded to the aromatic ring deformation. These observations confirm successful polymerization of aniline on the GO sheets. The mechanism of aniline polymerization on the GO sheets is schematically presented in **Figure 1.** It has been reported that the epoxide groups present on the GO surface are responsible for the oxidation of aniline. The aniline polymerization into PANI can take place at different steps as presented in **Figure 1**.

XRD patterns of the GO and GO-PANI are shown in **Figure 2b.** According to this figure an intensive characteristic diffraction peak (001) corresponding to an interlayer distance of d=10.22 Â can be seen at 2Θ=10.1°. This amount of interlayer distance resulted by the presence of oxygen containing groups i.e. hydroxyl, carboxylic and epoxy on the GO sheets.

The presence of broad peaks in PANI implies the existence of both amorphous and crystalline region [79]. On the other hand, XRD pattern of GO-PANI showed very sharp peak in comparison with PANI. This can be interpreted to highly ordered PANI's chains synthesized on the GO sheets [67].

Figure 2

DSC curves of both PANI and GO-PANI are depicted in **Figure 3**. Two distinct peaks can be distinguished for both samples. The first one (centered at 80-90 ^{o}C) is correlated to the water evaporation. The second one (centered at 210-240 ^{o}C) are correspondent to dopant loss and/or GO reduction (in the case of GO-PANI) [77, 78]. It should be noted that due to rigid chemical structure of PANI, it was not possible to detect its melting point before degradation.

Figure 3

The electrical conductivity of PANI was 70±10 $S.m^{-1}$ which is in accordance with previous reports [67, 76]. On the other hand, the electrical conductivity of GO-PANI was 530±40 $S.m^{-1}$. The possible mechanism for different electrical conductivity could be explained as the creation of common conductive pathway between GO (or rGO) and PANI which interplay as a bridge between two components [67]. Electrical conductivity of PANI is strongly dependent on its crystallinity [79]. In fact, ordered structure in PANI which results from doping process in Emeraldine oxidation state is responsible for charge transfer inside PANI's chains. Showing at least 7 fold higher electrical conductivity in GO-PANI sample suggests PANI's chains are highly ordered on the GO sheets [67]. These results are in high consistency with XRD measurements which exhibit highly crystalline structure (very sharp peaks) for PANI in GO-PANI sample.

3.2. GO and GO-PANI/ZRC properties characterization

3.2.1. OCP measurements

The cathodic protection behaviors of the ZRC, GO/ZRC and GO-PANI/ZRC samples can be compared through OCP measurements. The OCP values of these samples are shown in Fig.3 as a function of immersion time. From **Figure 4** it can be seen that the OCP values of the ZRC, GO/ZRC and GO-PANI/ZRC samples are below the OCP of iron (<-0.58 V (vs SCE)), indicating the effective cathodic protection capability of all coatings at the initial stage of immersion. Comparing the OCP values of different samples it can be seen that inclusion of GO and GO-PANI nanosheets into the ZRC resulted in the shift of OCP to less negative values, indicating the decrease of cathodic protection intensity at the first days of immersion. This is attributed to the effective barrier role of the nanosheets, decreasing the coating porosity and electrolyte diffusion rate. As the time progresses the OCP of the ZRC increases but the OCP of the GO/ZRC and GO-PANI/ZRC samples decreases. The increase of OCP of ZRC is attributed to the fast oxidation process of zinc particles, leading to zinc oxide corrosion products creation in the coating porosity, decreasing the zinc particles electrical contact and increasing the coating barrier performance. However, addition of GO and GO-PANI to the ZRC reduces the electrolyte diffusion rate and therefore zinc particles activation takes place at longer immersion times. The decrease in OCP is most pronounced for the GO-PANI/ZRC samples. This means that not only the barrier performance of the ZRC but also the electrical contact between the zinc particles and steel substrate can be remarkably improved after addition of GO-PANI, resulting in the increase of cathodic protection intensity of ZRC at long period of immersion. The conductive PANI nanofibers deposition on the GO surface provides proper barrier action and improves the electrical contact between the zinc particles. So the effective cathodic protection can be obtained for longer duration as a result of barrier role of GO sheets and conductive nature of PANI. The GO-PANI reduces the

electrolyte diffusion rate and in this way lower oxidation of zinc particles takes place during the exposure time. Moreover, the barrier properties improvements do not result in the coating sacrificial properties. These all show better cathodic protection properties of the GO-PANI/ZRC samples than GO-ZRC and ZRC samples. After about 55 days immersion the OCP of the ZRC became more positive than the OCP of iron, indicating no cathodic protection capability of this coating at long immersion time. However, the GO-ZRC and GO-PANI/ZRC samples show cathodic protection performance even at long immersion times. Compared to the GO/ZRC sample the GO-PANI/ZRC sample shows lower OCP (more negative) at long immersion time, indicating effective cathodic protection performance of this sample. Compared to the previous reports it can be seen that addition of barrier GO-PANI nanosheets to the ZRC could provide effective cathodic protection performance at long immersion times. After 50 days immersion the OCP of GO-PANI/ZRC sample shifted to less negative values. This can be attributed to both the zinc particle electrical contact loss as a result of zinc oxide creation and due to the redox properties of PANI-ES, catalyzing the formation of stable oxide layer (mainly based on Fe_3O_4) [74] on the steel surface.

Figure 4

3.2.2. Salt spray test results

The cathodic protection duration of the ZRC samples, before and after inclusion of 0.1 wt.% GO and GO-PANI nanosheets, was studied and compared by salt spray test. The test was performed on the samples with X-scribes at different exposure times of 500, 1000 and 2000 h (**Figure 5**). According to **Figure 5** white rust, composed of zinc oxide/hydroxide, covered the whole surface and filled the scribed areas of the ZRC samples after 500 h exposure time. There is no red corrosion rust in the scribed areas of the ZRC samples with GO and GO-PANI. However, the red rust slightly speared in the scribed areas on the ZRC sample without nanosheets. By increasing the exposure time up to 1000 and 2000 h red corrosion products

appeared in large amount at scribed regions, exhibiting poor cathodic protection performance of this coating at long exposure times. For the GO containing sample the first sing of red corrosion rust creation was observed at 1000 h and it became more visible after 2000 h exposure. However, compared to the ZRC coating it is clear that inclusion of GO nanosheets could remarkably enhance the sacrificial properties of the coating. It can be seen from the results that the red corrosion products were not observed on the ZRC sample filled with GO-PANI nanosheets at all exposure times, revealing the effective role of GO-PANI nanosheets on the ZRC cathodic protection properties enhancement. These observations reveal that inclusion of GO-PANI nanosheets into the ZRC could increase the sacrificial duration of the coating.

The adhesion strength of different samples was measured by pull-off test after 2000 h salt spray exposure. As can be seen from **Figure 5** the lowest adhesion strength was obtained for the ZRC sample. It is clear from the results that inclusion of GO and GO-PANI nanosheets resulted in the increase of adhesion strength. The highest adhesion strength values were obtained for the GO-PANI/ZRC sample. The coating detachment mechanism for all three samples was in the form of cohesive failure, depicting the poor coherency of the system as a result of the high zinc particles loading and zinc oxide corrosion products creation. It seems that salt spray test had more negative effect on the ZRC sample cohesion than GO and GO-PANI containing samples. This is due to the higher amount of zinc oxide creation in the coating and at the coating/steel interface, deteriorating the coating integrity and coherency.

Figure 5

3.2.3. SEM, EDS and XRD analyses

The surface morphology of ZRC, GO/ZRC and GO-PANI/ZRC samples before and after 500 and 1000 h salt spray test was studies by SEM analysis (**Figure 6**). The SEM micrographs of ZRC, GO/ZRC and GO-PANI/ZRC samples before salt spray test obviously show that the

spherical zinc particles are in contact with each other and the coatings are porous. After addition of GO, the GO sheets are located between the zinc particles and reduced the coating porosity. It can be seen that the ZRC, GO/ZRC and GO-PANI/ZRC samples surface morphology significantly changed after exposure to salt spray test condition. The spherical zinc particles oxidation resulted in zinc oxide corrosion products formation on the coating surface, resulting in the decrease of the coating porosity. The ZRC samples exposed to salt spray test for 1000 h show a dense and compacted morphology, indicating significant oxidation rate of zinc particles that adversely influenced its cathodic protection performance. For the GO containing sample the coating porosity was not increased as high as ZRC sample and the amount of corrosion products created were not the same as that of ZRC. After addition of GO-PANI nanosheets, the zinc particles oxidation noticeably decreased. The coating porosity did not significant change and the zinc particles had spherical morphology even after 1000 h salt spray test. Also, the form of oxidation of zinc particles is totally different from that of ZRC and GO-ZRC samples. XRD analysis was conducted to detect the phase composition of the ZRC, GO/ZRC and GO-PANI/ZRC samples after 1000 h salt spray test. The diffraction patterns of these samples are shown in **Figure 7**. Results show that $Zn(OH)_2$, ZnO, FeOOH and Fe_2O_3 are the main phases present in the XRD patterns of all samples. Compared to the ZRC sample the intensities of the diffraction peaks related to ZnO and $Zn(OH)_2$phases significantly decreased after addition of GO and GO-PANI nanosheets. In addition, the intensity of the peaks related to the FeOOH and Fe_2O_3 phases decreased after addition of GO-PANI, indicating good cathodic protection of this system, preventing the steel substrate from corrosion. The XRD results depict that inclusion of GO-PANI could noticeably reduce the oxidation rate of zinc particles and prevent the steel substrate from corrosion. Lower amount of zinc and iron oxides was detected by XRD analysis for the GO-PANI containing ZRC sample compared to the neat ZRC sample. These results are in

complete agreement with the previous experiments. To evaluate the surface composition of the ZRC, GO/ZRC and GO-PANI/ZRC samples the EDS spectra were obtained from the surface of these samples before and after 30 days immersion in 3.5 wt.% NaCl solution. From the results (**Figure 8 and Table 1**) O, Zn, C, N and Fe are the main elements detected on the surface of samples. The lowest oxidation of zinc particles in the GO-PANI/ZRC sample than others can be understood from the lower O and higher Zn contents on this sample compared to others. It can be seen from the results that the O content of the ZRC samples significantly increased after immersion in chloride solution, indicating zinc oxide/hydroxide creation [75]. In addition, no Fe was detected on the surface of this sample, indicating that addition of GO-PANI nanosheets could successfully enhance the cathodic protection properties of ZRC and protect the steel substrate from corrosion.

Figure 6

Figure 7

Figure 8

Table 1

As depicted in **Figure 9** the HR-TEM image clearly demonstrate the PANI nanofibers deposition on the GO sheets. The FE-SEM micrographs also confirm the GO nanosheets dispersion in the ZRC matrix. It can be seen from the FE-SEM micrographs that the GO sheets properly dispersed in the coating matrix and reduced the coating porosity. As it is schematically shown in this figure the PANI-GO sheets can remarkably reduce the coating porosity due to the high specific surface area of the GO sheets, leading to the coating barrier properties enhancement. In addition, the PANI nanofibers can increase the zinc particles electrical contact, leading to the coating cathodic protection properties improvement. As shown in **Figure 10** the spongy morphology of zinc particles confirms the role of PANI nanofibers on enhancing the coating cathodic protection behavior. The PANI nanofibers

connect the zinc particles to each other even when the zinc oxides fill the coating porosity at long exposure times. The regions of the zinc surface connected to PANI can be oxidized faster than other parts due to better electron transfer, leading to a spongy surface morphology.

Figure 9

Figure 10

3.2.3. EIS analysis

The corrosion protection performance of the steel panels coated with ZRC GO/ZRC and GO-PANI/ZRC was examined by EIS analysis after 10, 30 and 50 days immersion in 3.5 wt.% NaCl solution (**Figure 11 and 12**). Impedance at low frequency ($|Z|_{10\ mHz}$) and phase angle at high frequency ($\Theta_{10\ kHz}$) values were obtained from Bode diagrams (**Figure 13**). It can be seen from **Figures 11, 12 and 13** that the $|Z|_{10\ mHz}$ for the ZRC sample is near 10 kohm cm^2 after 10 days immersion but the$|Z|_{10mHz}$ increased dramatically after 30 and 50 days immersion. The ZRC has porous structure that is conductive pathways for corrosive agents. The zinc particles are electrically in contact with each other and steel substrate, providing an electron pathway from the surface of ZRC to the steel substrate. Very low $|Z|_{10\ mHz}$ value of the ZRC during the early stages of immersion depicts that the ZRC could provide effective cathodic protection through sacrificial role of the zinc particles. However, the $|Z|_{10\ mHz}$ remarkably increased after 30 days immersion, exhibiting significant reduction of the cathodic protection behavior of the ZRC. As the immersion time progresses the zinc particles convert to zinc oxide/hydroxide, leading to the particles electrical contacts reduction. As a result, the coating cathodic protection capability decreases and its barrier role increases. The increase of barrier action is mainly due to the decrease of the coating porosity which resulted by the zinc oxide creation between the zinc particles. From **Figure 13a** it can be seen that addition of GO to the ZRC sample resulted in the greater $|Z|_{10\ mHz}$ value than ZRC sample after 10 days immersion. It is known that a monolayer graphene sheet is impermeable to all

gases and water molecules. So due to the high surface area of the GO nanosheets they provide excellent barrier properties against oxygen and water diffusion. Incorporation of GO nanosheets into the ZRC enhanced its barrier properties through filling the porosities. This can be seen from the higher $|Z|_{10\ mHz}$ values of the GO-ZRC sample than ZRC after 10days immersion. Unlike ZRC the $|Z|_{10\ mHz}$of the GO-ZRC sample did not significantly change after 30 and 50 days immersion. This means that addition of GO nanosheets to ZRC enhanced the cathodic protection duration and reduced the zinc particles oxidation rate through decreasing the porosity index and electrolyte diffusion rate. However, the GO sheets could partially reduce the electrical connection of zinc-zinc particles and zinc particles-steel substrate. So this is resulted in slight decrease of sacrificial behavior of the coating. To overcome this problem, GO-PANI was added to ZRC. The PANI nanofibers deposited on the GO sheets are mostly in the form of Emeraldine salt (PANI-ES) which shows conductive properties [63]. The PANI-ES can be easily converted to the Emeraldine base (PANI-EB) through capturing the electrons released as a result of the zinc particles oxidation ($Zn \rightarrow Zn^{2+}+2e$). In the presence of Cl^-ions present in the corrosive electrolyte the PANI-EB can be again converted to the PANI-ES, completing the autocatalytic cycle. These can result in the stabilization of Fe in the passive region and zinc in its active form [63]. As depicted in **Figure 13,** the $|Z|_{10\ mHz}$ of the ZRC drastically decreased after addition of GO-PANI compared to the ZRC and GO-ZRC samples. However, the increase of$|Z|_{10\ mHz}$ can be seen after 30 and 50 days immersion. The significant decrease in $|Z|_{10\ mHz}$ of the GO-PANI/ZRC sample is related to the conducting role of PANI fibers deposited on the GO sheets. The GO-PANI sheets provide barrier against water and oxygen but enhances the electrical connection of the zinc particles. So the PANI fibers deposited on the GO sheets connect the zinc particles and in this way provide new electrical conduction pathways in the ZRC. As a result, the sacrificial behavior of the ZRC can be noticeably improved. As the time progresses the zinc

particles oxidation results in the increase of the coating barrier properties enhancement. After 30 days immersion, the barrier role of the GO-PANI particles is dominant but the sacrificial behavior of the ZRC is still high due to the PANI role of enhancing the zinc particles electrical connection even when there are zinc oxide products in the coating structure. These observations are in accordance with the salt spray and SEM results. The barrier role of GO and conductive behavior of PANI result in the creation of ZRC system with higher cathodic protection duration.

Figure 11

Figure 12

Figure 13

4. Conclusions

A highly cystalline and conductive GO-PANI composite was synthesized and characterized. The effect of GO and GO-PANI on the corrosion protection performance and mechanism of ZRC was compared. The main results obtained are listed below:

- FT-IR, XRD and HR-TEM analyses confirmed that the highly crystalline and conductive polyaniline (PANI) nanofibers synthesized on the GO surface through an in situ polymerization of aniline in the presence of GO as an oxidant. The PANI deposited on the GO surface in this method is mostly attached in the chemical form rather than physical form, leading to lower negative effects on the ZRC coating mechanical and adhesion properties.
- OCP, SEM and salt spray test results depicted the enhanced barrier properties and cathodic protection duration of the ZRC after addition of GO and GO-PANI nanosheets. It was shown that inclusion of GO into the ZRC could improve the ZRC performance only through enhancing its barrier properties without disturbing the zinc particles electrical contact. On the other hand, the GO-PANI provided additional

effect and remarkably improved the electrical contact of zinc particles and steel substrate, leading to longer protection service life.

- EIS results showed proper cathodic protection properties of the ZRC samples loaded with GO-PANI at early stage and after long exposure times. Compared to the conventional nanoparticles the GO-PANI behaved as a good corrosion protection modifier of GO. PANI also could reduce the zinc particles oxidation without disturbing theirs electrical contact.

References

[1] F. Tang, G. Chen, R.K. Brow, J.S. Volz, M.L. Koenigstein, Corrosion resistance and mechanism of steel rebar coated with three types of enamel, Corros Sci 59 (2012) 157-168.

[2] S. Pour-Ali, C. Dehghanian, A. Kosari, Corrosion protection of the reinforcing steels in chloride-laden concrete environment through epoxy/polyaniline–camphor sulfonate nano composite coating, Corrs Sci 90 (2015) 239-247.

[3] K. Saravanan, S. Sathiyanarayanan, S. Muralidharan, S.S. Azim, G. Venkatachari, Performance evaluation of polyaniline pigmented epoxy coating for corrosion protection of steel in concrete environment, Prog Org Coat 59 (2007) 160-167.

[4] Z. Wang, E. Han, F. Liu, Z. Qian, L. Zhu, Waterborne epoxy nanocoatings modified by nanoemulsions and nanoparticles, J. Mater. Sci. Technol 30 (2014) 1036-1042.

[5] H. Shi, F. Liu, E. H. Han, Surface-engineered microcapsules by layer-by-layer assembling for entrapment of corrosion inhibitor, J. Mater. Sci. Technol. 31 (2015) 512-516.

[6] S. Gonzalez, F. Caceres, V. Fox, R.M. Souto, Resistance of metallic substrates protected by an organic coating containing aluminium powder, Prog Org Coat 46 (2003) 317–23.

[7] B.Ramezanzadeh, M.Khazaei, A.Rajabi, G.Heidari, D.Khazaei, Corrosion resistance and cathodic delamination of an epoxy/polyamide coating on milled steel, Corrosion 70(1) (2014) 57–65.

[8] B.Nikravesh, B.Ramezanzadeh, A.A.Sarabi, S.M.Kasirih, Evaluation of the corrosion resistance of an epoxy-polyamide coating containing different ratios of micaceous iron oxide/Al pigments, Corros Sci 53 (2011) 1592–603.

[9] M.Mahdavian, M. Attar, Evaluation of zinc phosphate and zinc chromate effectiveness via AC and DC methods, Prog Org Coat 53 (2005) 191–4.

[10] A.C.Bastos, M.G.Ferreira, A.M.Simoes, Corrosion inhibition by chromate and phosphate extracts for iron substrates studied by EIS and SVET, Corros Sci 48(6) (2006) 1500–12.

[11] B. Ramezanzadeh, S. Y. Arman, M. Mehdipour, Anticorrosion properties of an epoxy zinc-rich composite coating reinforced with zinc, aluminum, and iron oxide pigments, J. Coat. Technol. Res 11 (5) (2014) 727–737.

[12] H. Marchebois, M. Keddam, C. Savall, J. Bernard, S. Touzain, Electrochemical behavior of zinc-rich powder coatings in artificial sea water, Electrochim. Acta17 (18) (2004) 2945–2954.

[13] S.Y. Arman, B. Ramezanzadeh, S. Farghadani, M. Mehdipour, A. Rajabi, Application of the electrochemical noise to investigate the corrosion resistance of an epoxy zinc-rich coating loaded with lamellar aluminum and micaceous iron oxide particles, Corros Sci 77 (2013) 118–127

[14] M.M. Ahadi, M.M. Attar, OCP measurement: a method to measure CPVC, Sci.Iran 14 (2007) 369–372.

[15] M.E. Nanna, G.P. Bierwagen, Mg-rich coatings: a new paradigm for Cr-free corrosion protection of Al aerospace alloys, JCT Res. 1 (2004) 69–80.

[16] A. Kalendova, Effects of particle sizes and shapes of zinc metal on the properties of anticorrosive coatings, Prog. Org. Coat. 46 (4) (2003) 324–332.

[17] D. Loveday, P. Peterson, B. Rodgers, Gamry instruments, J. Coat. Technol (2005) 22.

[18] V. Barranco, S. Feliu Jr., S. Feliu, EIS study of the corrosion behavior of zinc based coatings on steel in quiescent 3% NaCl solution. Part 1: directly exposed coatings, Corros. Sci. 46 (2004) 2203–2220.

[19] S. Shreepathi, P. Bajaj, B.P. Mallik, Electrochemical impedance spectroscopy investigations of epoxy zinc rich coatings: role of Zn content on corrosion protection mechanism, Electrochim. Acta 55 (2010) 5129–5134.

[20] A. Meroufel, C. Deslouis, S. Touzain, Electrochemical and anticorrosion performances of zinc-rich and polyaniline powder coatings, Electrochim.Acta 53 (2008) 2331–2338.

[21] K. Schaefer, A. Miszczyk, Improvement of electrochemical action of zinc-rich paints by addition of nanoparticulate zinc, Corros. Sci. 66 (2013) 380–391.

[22] N. Arianpouya, M. Shishesaz, A. Ashrafi, Evaluation of synergistic effect of nanozinc/nanoclay additives on the corrosion performance of zinc-rich polyurethane nanocomposite coatings using electrochemical properties and salt spray testing, Surf. Coat. Technol. 216 (2013) 199‑206.

[23] R.N. Jagtap, P.P. Patil, S.Z. Hassan, Effect of zinc oxide in combating corrosion in zinc-rich primer, J. Prog. Org. Coat. 63 (2008) 389‑394.

[24] L. Zhang, A. Ma, J. Jiang, D. Song, Anti-corrosion performance of waterborne Zn rich coating with modified silicon-based vehicle and lamellar Zn (Al) pigments, Prog. Natur. Sci: Mater. Int. 22 (4) (2012) 326‑333.

[25] A. Gergely, Pfeifer, I. Bertóti, T. T̨r̨ok, E. K̨lm̨n, Corrosion protection ofcold-rolled steel by zinc-rich epoxy paint coatings loaded with nano-sizealumina supported polypyrrole, Corros. Sci. 53 (11) (2011) 3486‑3499.

[26] M. Jalili, M. Rostami, B. Ramezanzadeh, An investigation of the electrochemical action of the epoxy zinc-rich coatings containing surface modified aluminum nanoparticle, Appl Surf Sci 328 (2015) 95–108

[27] Y. Cubides H. Castaneda, Corrosion protection mechanisms of carbon nanotube and zinc-rich epoxy primers on carbon steel in simulated concrete pore solutions in the presence of chloride ions, Corros Sci doi:10.1016/j.corsci.2016.03.023

[28] E. Akbarinezhad, M. Ebrahimi, F. Sharif, A. Ghanbarzadeh, Evaluating protection performance of zinc rich epoxy paints modified with polyaniline and polyaniline-clay nanocomposite, Prog. Org. Coat. 77 (2014) 1299-1308.

[29] F. Tohidi Shirehjini, I.Danaee, H.Eskandari, D.Zarei, Effect of Nano Clay on Corrosion Protection of Zinc-Rich Epoxy Coatings on Steel 37, Journal of Materials Science &Technology doi: 10.1016/j.jmst.2016.08.017

[30] A. Anandhi, S. Palraj, G. Subramanian, M. Selvaraj, Corrosion resistance and improved adhesion properties of propargyl alcohol impregnated mesoporous titanium dioxide built-in epoxy zinc rich primer, Prog Org Coat 97 (2016) 10-18

[31] T.Ho Yun, J.Hoon Park, J-S.Kim, J.Myung Park, Effect of the surface modification of zinc powders with organosilanes on the corrosion resistance of a zinc pigmented organic coating, Prog Org Coat 77 (11) (2014) 1780-1788

[32] K.S. Novoselov, A.K. Geim, S.V. Morozov, D. Jiang, Y. Zhang, S.V. Dubonos, et al., Electric field effect in atomically thin carbon films, Science 306 (2004) 666–669.

[33] K.S. Novoselov, A.K. Geim, S.V. Morozov, D. Jiang, M.I. Katsnelson, I.V.Grigorieva, et al., Two-dimensional gas of massless Dirac fermions in graphene, Nature 438 (2005) 197–200.

[34] N. Tombros, C. Jozsa, M. Popinciuc, H.T. Jonkman, B.J. Van Wees, Electronic spin transport and spin precession in single graphene layers at room temperature, Nature 448 (2007) 571–574.

[35] F. Ji, Y.L. Li, J.M. Feng, D. Su, Y.Y. Wen, Y. Feng, et al., Electrochemical performance of graphene nanosheets and ceramic composites as anodes forlithium batteries, J. Mater. Chem. 19 (2009) 9063–9067.

[36] A.A. Balandin, S. Ghosh, W.Z. Bao, I. Calizo, D. Teweldebrhan, F. Miao, et al., Superior thermal conductivity of single-layer graphene, Nano Lett. 8 (2008)902–907.

[37] Y. Zhang, Y.-W. Tan, H.L. Stormer, P. Kim, Experimental observation of the quantum Hall effect and Berry's phase in graphene, Nature 438 (7065) (2005)201–204.

[38] C. Lee, X. Wei, J.W. Kysar, J. Hone, Measurement of the elastic properties and intrinsic strength of monolayer graphene, Science 321 (5887) (2008) 385–388.

[39] D.A. Dikin, S. Stankovich, E.J. Zimney, R.D. Piner, G.H.B. Dommett, G.Evmenenko, et al., Preparation and characterization of graphene oxide paper, Nature 448 (2007) 457–460.

[40] S. Stankovich, D.A. Dikin, G.H.B. Dommett, K.M. Kohlhaas, E.J. Zimney, E.A.Stach, et al., Graphene-based composite materials, Nature 442 (2006) 282–286.

[41] B. Ramezanzadeh, E. Ghasemi, M. Mahdavian, E. Changizi, M.H. Mohamadzadeh Moghadam, Characterization of covalently-grafted polyisocyanate chains onto graphene oxide for polyurethane composites with improved mechanical properties, Chem Eng J 281 (2015) 869–883

[42] A.Ahmadi, B. Ramezanzadeh, M.Mahdavian, Hybrid silane coating reinforced with silanized graphene oxide nanosheets with improved corrosion protective performance, RSC Adv 6 (2016) 54102–54112

[43] B. Ramezanzadeh, A. Ahmadi, M. Mahdavian, Enhancement of the corrosion protection performance and cathodic delamination resistance of epoxy coating through treatment of steel

substrate by a novel nanometric sol-gel based silane composite film filled with functionalized graphene oxide nanosheets, Corros Sci 109 (2016) 182–205

[44] B. Ramezanzadeh, S. Niroumandrad, A. Ahmadi, M. Mahdavian, M.H. Mohamadzadeh Moghadam, Enhancement of barrier and corrosion protection performance of an epoxy coating through wet transfer of amino functionalized graphene oxide, Corros Sci 103 (2016) 283–304

[45] B. Ramezanzadeh, Z. Haeri, M. Ramezanzadeh, A facile route of making silica nanoparticles-covered graphene oxide nanohybrids (SiO2-GO); fabrication of SiO2-GO/epoxy composite coating with superior barrier and corrosion protection performance, Chem Engin J 303 (2016) 511–528

[46] D.Liu, W.Zhao, S.Liu, Q.Cen, Q.Xue, Comparative tribological and corrosion resistance properties of epoxy composite coatings reinforced with functionalized fullerene C60 and graphene, Surf Coat Technol 286 (2016) 354-364

[47] J.Li, J.Cui, J.Yang, Y.Ma, H.Qiu, J.Yang, Silanized graphene oxide reinforced organofunctional silane composite coatings for corrosion protection, Prog Org Coat 99 (2016) 443-451

[48] S.Liu, L.Gu, H.Zhao, J.Chen, H.Yu, Corrosion Resistance of Graphene-Reinforced Waterborne Epoxy Coatings, J Mater Sci Technol 32 (5) (2016) 425-431

[49] D.Liu, W.Zhao, S.Liu, Q.Cen, Q.Xue, Comparative tribological and corrosion resistance properties of epoxy composite coatings reinforced with functionalized fullerene C60 and graphene, Surf Coat Technol 286 (2016) 354-364

[50] J.Li, J.Cui, J.Yang, Y.Ma, H.Qiu, J.Yang, Silanized graphene oxide reinforced organofunctional silane composite coatings for corrosion protection, Prog Org Coat 99 (2016) 443-451

[51] S.Liu, L.Gu, H.Zhao, J.Chen, H.Yu, Corrosion Resistance of Graphene-Reinforced Waterborne Epoxy Coatings, J Mater Sci Technol32 (5) (2016) 425-431

[52] Z. Yu, H. Di, Y. Ma, Y. He, L. Liang, L. Lv, X. Ran, Y. Pan, Z. Luo, Preparation ofgraphene oxide modified by titanium dioxide to enhance the anti-corrosion performance of epoxy coatings, Surf. Coat. Technol. 276 (2015) 471-478.

[53] M. Mo, W. Zhao, Z. Chen, Q. Yu, Z. Zeng, X. Wu, Q. Xue, Excellent tribologicaland anti-corrosion performance of polyurethane composite coatings reinforced with functionalized graphene and graphene oxide nanosheets, RSC Adv. 5 (70) (2015) 56486–56497.

[54] H.Di, Z.Yu, Y.Ma, C.Zhang, F.Li, L.Lv, Y.Pan, H.Shi, Y.He, Corrosion-resistant hybrid coatings based on graphene oxide–zirconia dioxide/epoxy system, Journal of the Taiwan Institute of Chemical Engineers 67 (2016) 511–520

[55] Z.Yu, H.Di, Y.Ma, L.Lv, Y.Pan, C.Zhang, Y.He, Fabrication of graphene oxide–alumina hybrids to reinforce the anti-corrosion performance of composite epoxy coatings, Appl Surf Sci 51 (2015) 986-996

[56] D.Liu, W.Zhao, S.Liu, Q.Cen, Q.Xue, Comparative tribological and corrosion resistance properties of epoxy composite coatings reinforced with functionalized fullerene C60 and graphene, Surf Coat Technol 286 (2016) 354-364

[57] J.Li, J.Cui, J.Yang, Y.Ma, H.Qiu, J.Yang, Silanized graphene oxide reinforced organofunctional silane composite coatings for corrosion protection, Prog Org Coat 99 (2016) 443-451

[58] S.Liu, L.Gu, H.Zhao, J.Chen, H.Yu, Corrosion Resistance of Graphene-Reinforced Waterborne Epoxy Coatings, J Mater Sci Technol 32 (2016) 425-431.

[59] B.P. Singh, B.K. Jena, S. Bhattacharjee, L.Besra, Development of oxidation and corrosion resistance hydrophobic graphene oxide-polymer composite coating on copper, Surf Coat Technol 232 (2013) 475–81.

[60] N.T. Kirkland, T. Schiller, N. Medhekar, N. Birbilis, Exploring graphene as a corrosion protection barrier, Corros Sci56 (2012) 1–4.

[61] K.R. Ratinac, W. Yang, J.J. Gooding, P. Thordarson, F. Braet, Graphene and related materials in electrochemical sensing, Electroanalysis 23(4) (2011) 803–26.

[62] K-C. Chang, M-H. Hsu, H-I. Lu, M-C. Lai, P-J. Liu, C-H. Hsu, et al. Room-temperature cured hydrophobic epoxy/graphenecomposites as corrosion inhibitor for cold-rolled steel. Carbon 6(6) (2014) 144–53.

[63] J.I. Martins, T.C. Reis, M. Bazzaoui, E.A. Bazzaoui, L.I. Martins, The effect of pH on the pyrrole electropolymerization on iron in malate aqueous solutions, Pro Org Coat65 (1) (2009) 62-70.

[64] N.A. Ogurtsov, A.A. Pud, P. Kamarchik, G.S. Shapoval, Corrosion inhibition of aluminum alloy in chloride mediums by undoped and doped forms of polyaniline, Synth. Met. 143 (2004)43-47.

[65] E. Armelin, M. Marti, F. Liesa, J.I. Iribarren, C. Aleman, Partial replacement of metallic zinc dust in heavy duty protective coatings by conducting polymer, Prog. Org. Coat. 69 (2010) 26–30.

[66] H.C. Schniepp, J.L. Li, M.J. McAllister, H. Sai, M. Herrera-Alonso, D.H. Adamson, et al., Functionalized single graphene sheets derived from splitting graphite oxide, J. Phys. Chem. B 110 (17) (2006) 8535–8539.

[67] M.H.Mohamadzadeh Moghadam, S.Sabury, M.Moazzami Gudarzi, F.Sharif, Graphene Oxide-Induced Polymerization and Crystallization to Produce Highly Conductive

Polyaniline/Graphene Oxide Composite, JOURNAL OF POLYMER SCIENCE, PART A: POLYMER CHEMISTRY 52 (2014) 1545–1554

[68] M. Trchov, I.Sedenkov, E. Tobolkov, J. Stejskal, FTIR spectroscopic and conductivity study of the thermal degradation of polyaniline films, Polym. Degrad. Stab 86 (2004) 179–185.

[69] M. Trchova, J. Stejskal, J. Proke, Infrared spectroscopic study of solid-state protonation and oxidation of polyaniline, Synth. Metals 101 (1999) 840–841.

[70] T. Fukuda, H. Takezoe, K. Ishikawa, A. Fukuda, H. S. Woo, S. K. Jeong, E. J. Oh, J. S. Suh, Ir and Raman studies in three polyanilines with different oxidation level, Synth. Metals 69 (1995) 175–176.

[71] M. Trchova, J. Stejskal, Polyaniline: The infrared spectroscopy of conducting polymer nanotubes (IUPAC Technical Report), Pure Appl. Chem. 83 (2011) 1803–1817.

[72] M. Ohira, T. Sakai, M. Takeuchi, Y. Kobayashi, M. Tsuji, Raman and infrared spectra of polyaniline, Synth. Metals 18 (1987) 347–352.

[73] C.-M. Chen, J.-Q. Huang, Q. Zhang, W.-Z. Gong, Q.-H. Yang, M.-Z. Wang, Y.-G. Yang, Annealing a graphene oxide film to produce a free standing high conductive graphene film, Carbon 50 (2012) 659–667.

[74] W-K.Lu, R.L. Elsenbaumer, B.Wessling, Corrosion Protection Of Mild Steel By Coatings Containing Polyaniline, Synthetic Metals 71 (1995) 2163-2166

[75] Y. Cubides, H. Castaneda, Corrosion protection mechanisms of carbon nanotube and zinc-rich epoxy primers on carbon steel in simulated concrete pore solutions in the presence of chloride ions, Corros Sci 109 (2016) 145-161.

[76] Y. Cao, A. Andreatta, A. J. Heeger, P. Smith, Influence of chemical polymerization conditions on the properties of polyaniline, Polymer 30 (1989) 2305-2311.

[77] W.F. Alves, E.C.Venancio, F.L.Leite, D.H.Kanda, L.F. Malmonge, J.A. Malmonge, L.H.Mattoso, Thermo-analyses of polyaniline and its derivatives. *Thermochimica Acta* 502 (2010), 43-46.

[78] M.Zilberman, G. I. Titelman, A. Siegmann, Y. Haba, M. Narkis, and D. Alperstein, Conductive blends of thermally dodecylbenzene sulfonic acid-doped polyaniline with thermoplastic polymers, Journal of Applied Polymer Science 66 (1997) 243-253.

[79] J. P. Pouget, M. E. Jdzefowicz, A. J. Epstein, X. Tang, A. G. MacDiarmid, X-ray Structure of Polyaniline, Macromolecules 24 (1991) 779-89.

[80] M.M.Gudarzi, M.H.M. Moghadam, F. Sharif, Spontaneous exfoliation of graphite oxide in polar aprotic solvents as the route to produce graphene oxide–organic solvents liquid crystals. Carbon, 64 (2013) 403-415.

Figure captions:

Figure 1- Schematic representation of GO and GO-PANI synthesis procedure

Figure 2- (a) FT-IR spectra and (b) XRD patterns of the GO and GO-PANI samples

Figure 3- DSC thermograms of the PANI and GO-PANI samples

Figure 4- OCP vs SCE for the ZRC, GO/ZRC and GO-PANI/ZRC samples after diffeftrrt immersion times.

Figure 5- Visual observations of the ZRC, GO/ZRC and GO-PANI/ZRC samples after 500, 1000 and 2000 h exposure to salt spray test condition, pull-off test results after 2000 h salt spray test

Figure 6- FE-SEM micrographs of the ZRC, GO/ZRC and GO-PANI/ZRC samples after 0, 500 and 1000 h exposure to salt spray test condition

Figure 7- XRD patterns of the ZRC, GO/ZRC and GO-PANI/ZRC samples after 1000 h exposure to salt spray test

Figure 8- EDS spectra of the ZRC, GO/ZRC and GO-PANI/ZRC samples after 30 days immersion in 3.5 wt.% NaCl solution

Figure 9- (a) High magnification FE-SEM micrographs of the GO-PANI/ZRC sample; (b) HR-TEM micrograph of GO-PANI, (c) schematic representation of the effect of GO-PANI on the ZRC performance

Figure 10- High magnification FE-SEM micrographs of the GO-PANI/ZRC sample after 1000 h salt spray test; schematic representation of the effect of GO-PANI on the zinc particles oxidation mechanism

Figure 11- Nyquist and Bode diagrams of the ZRC sample after 10, 10 and 50 days immersion in 3.5 wt.% NaCl solution

Figure 12- Nyquist and Bode diagrams of the (a_1 and a_2) GO-ZRC, and (b_1 and b_2) GO-PANI/ZRC samples after 10, 30 and 50 days immersion in 3.5 wt.% NaCl solution

Figure 13. (a) The values of impedance at 10 mHz and (b) phase angle at 10 kHz obtained from Bode diagrams after 10, 30 and 50 days immersion in 3.5 wt.% NaCl solution

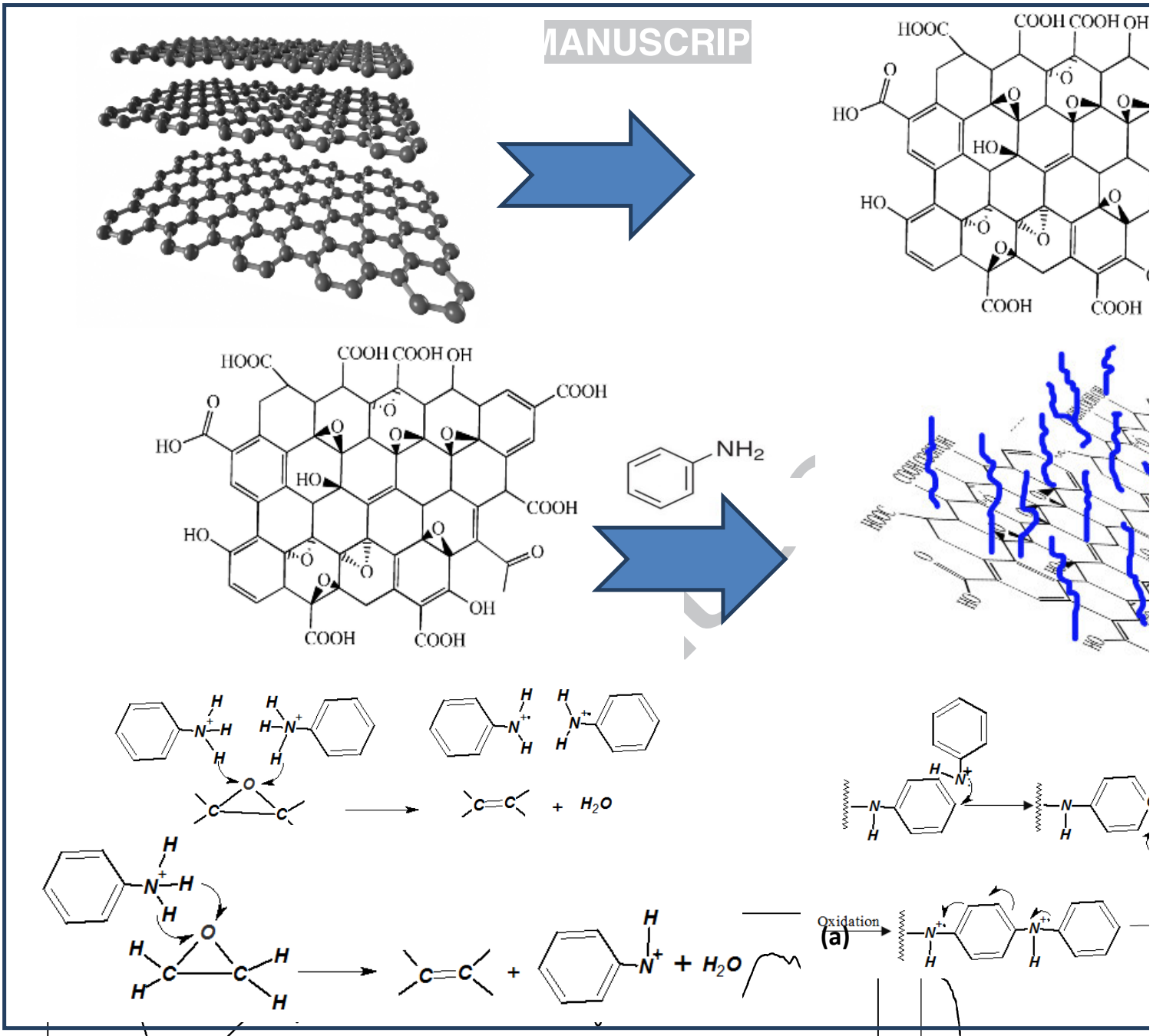

Figure 1- Schematic representation of GO and GO-PANI synthesis procedure

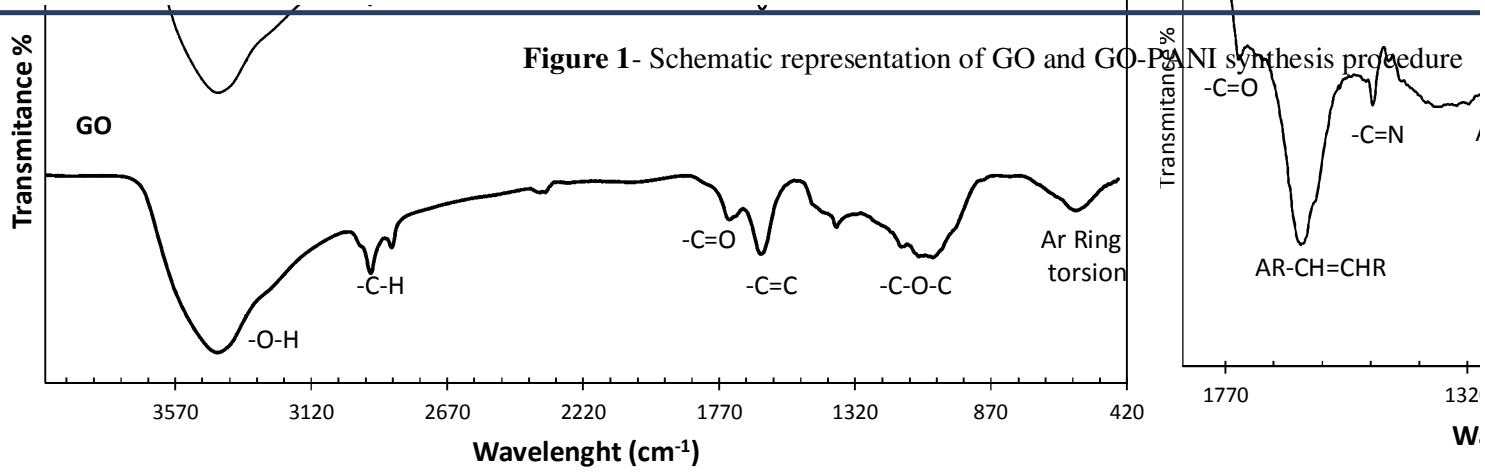

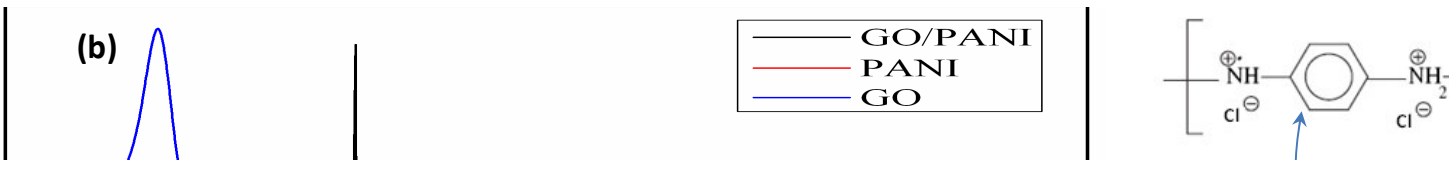

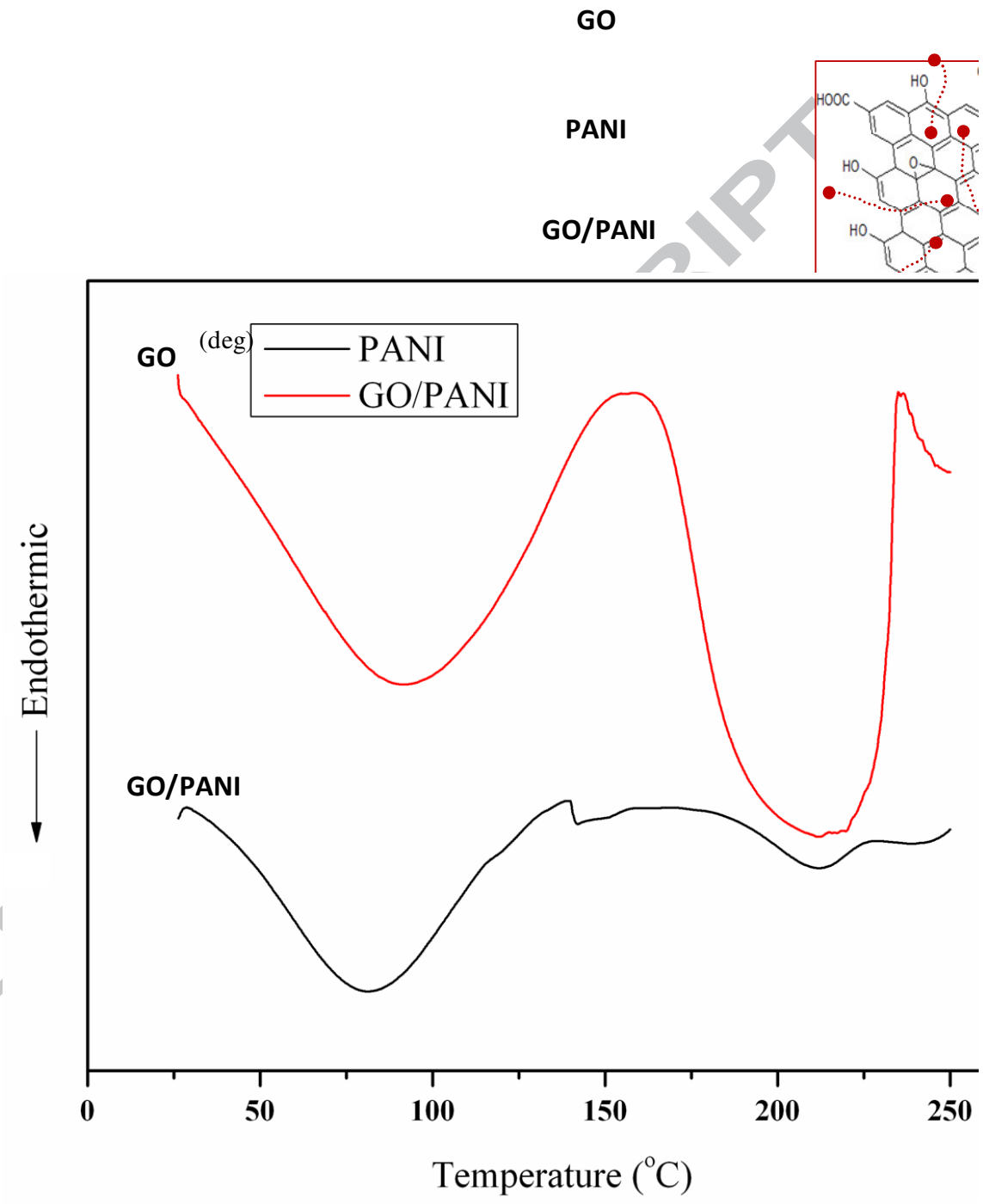

Figure 4- OCP vs SCE for the ZRC, GO/ZRC and GO-PANI/ZRC samples after diffeftrrt

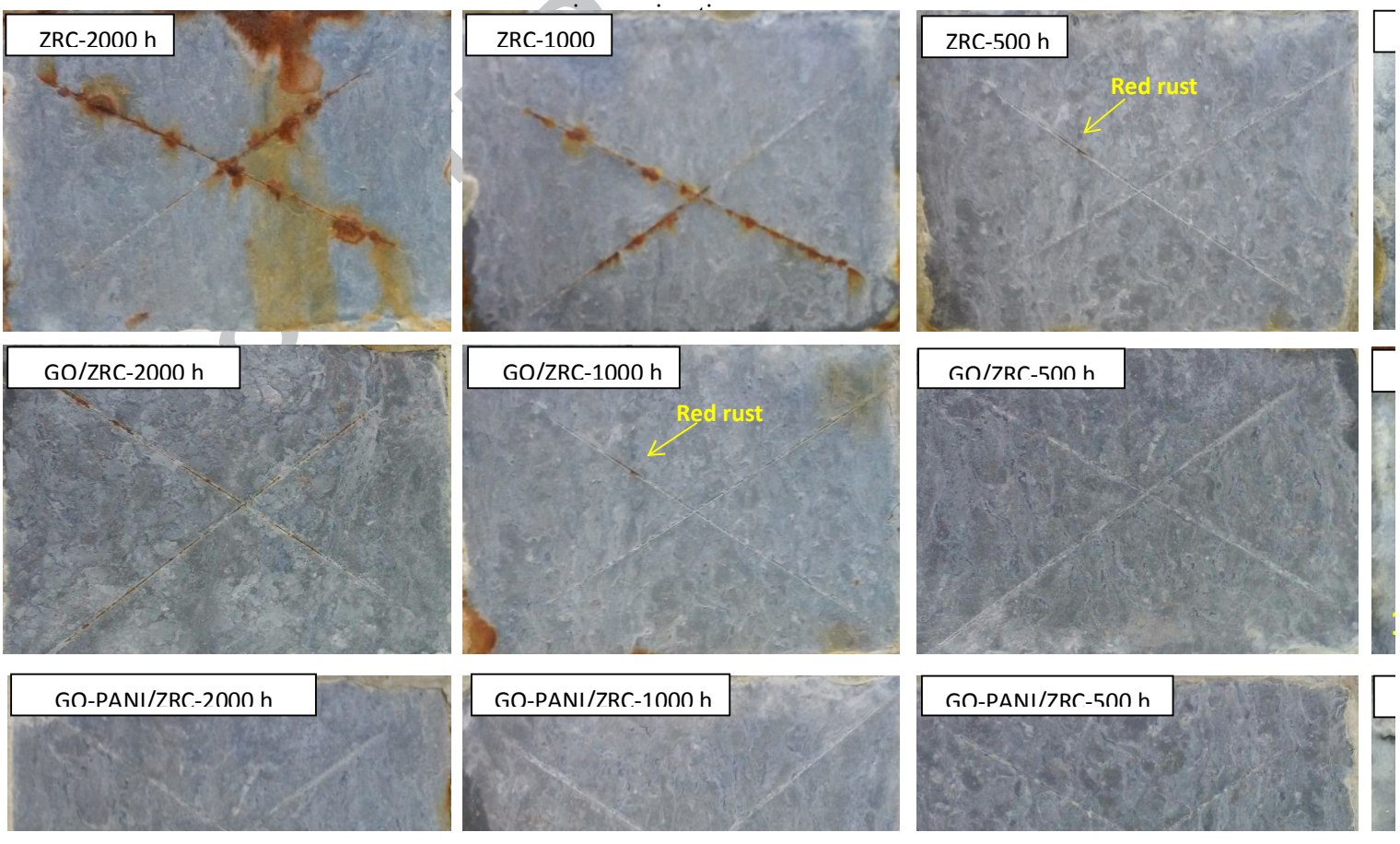

Fig
10
R
it
st

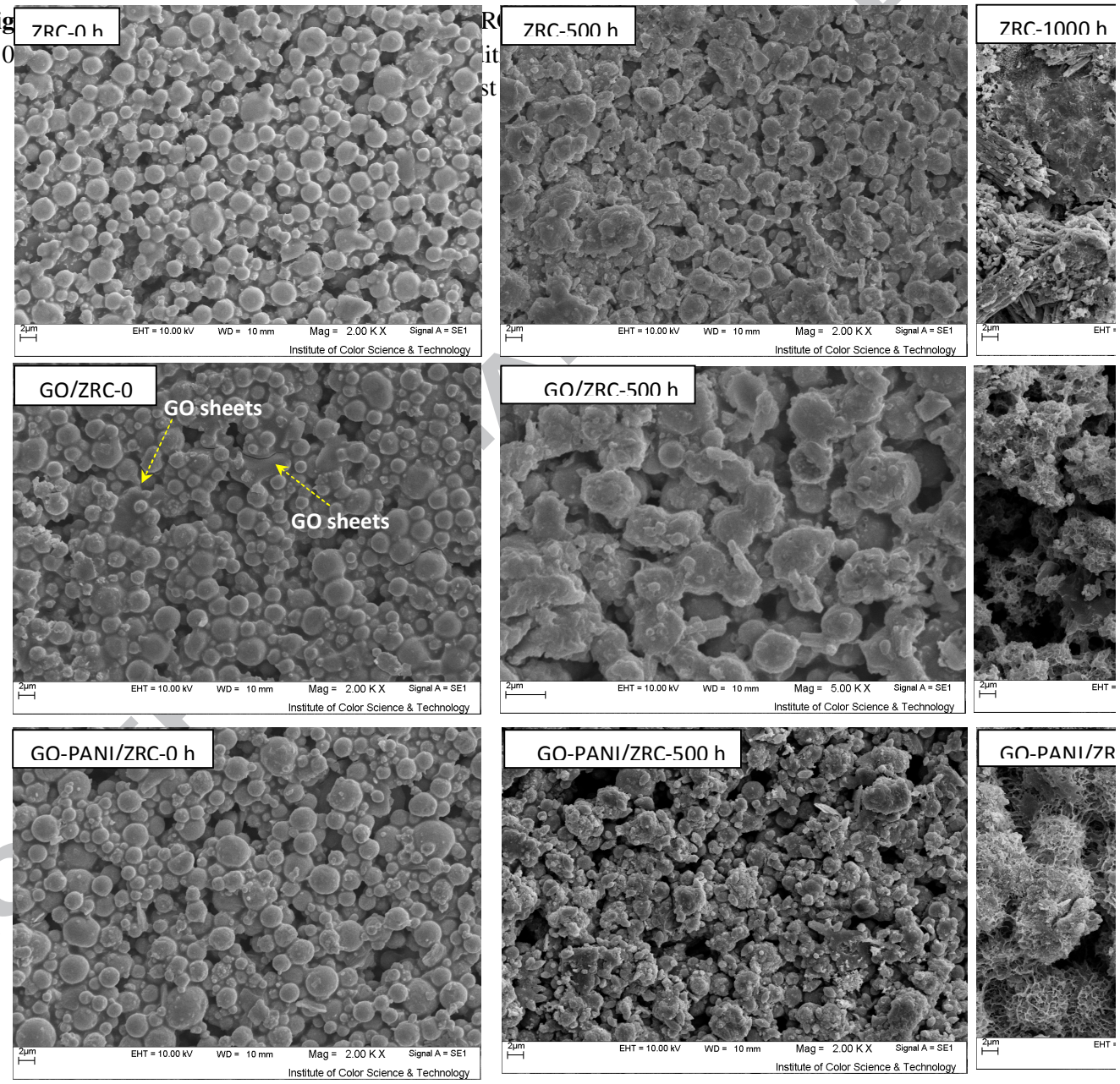

Figure 6- FE-SEM micrographs of the ZRC, GO/ZRC and GO-PANI/ZRC samples after 0, 500 and 1000 h

7000

6000

ZRC

GO-PANI/ZRC

GO/ZRC

Figu **ZI**

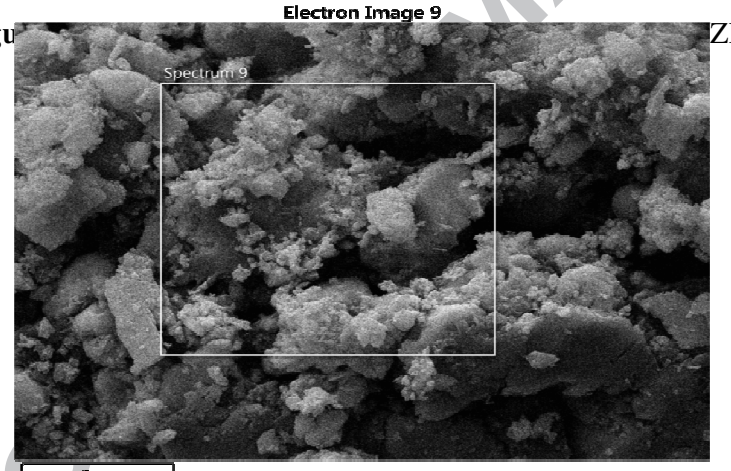

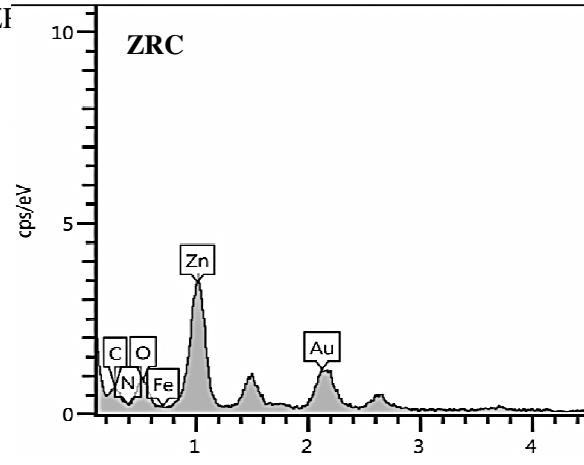

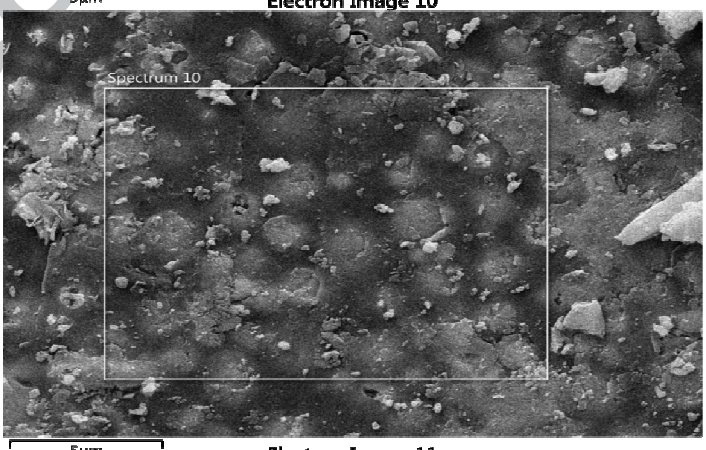

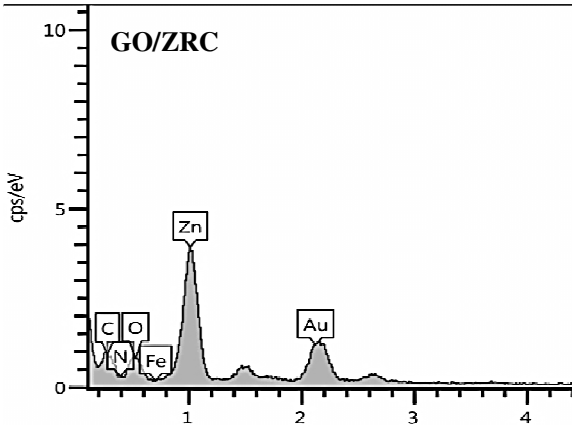

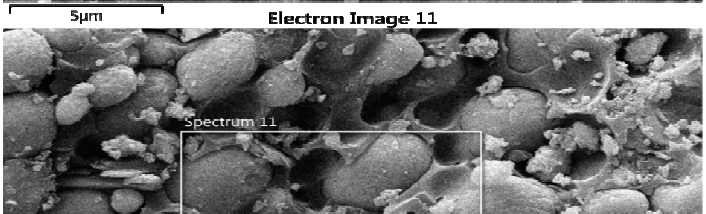

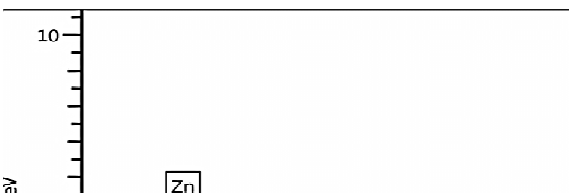

GO-PANI/ZRC

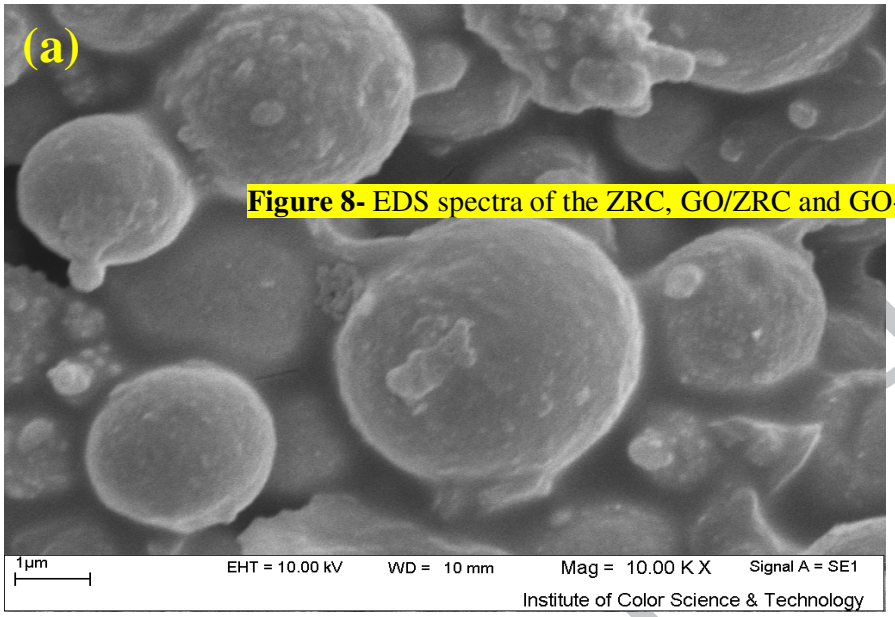

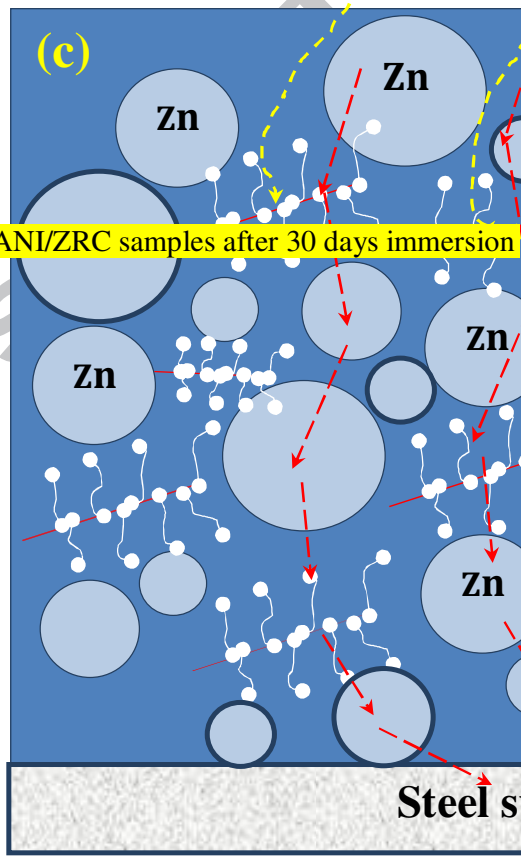

Figure 8- EDS spectra of the ZRC, GO/ZRC and GO-PANI/ZRC samples after 30 days immersion

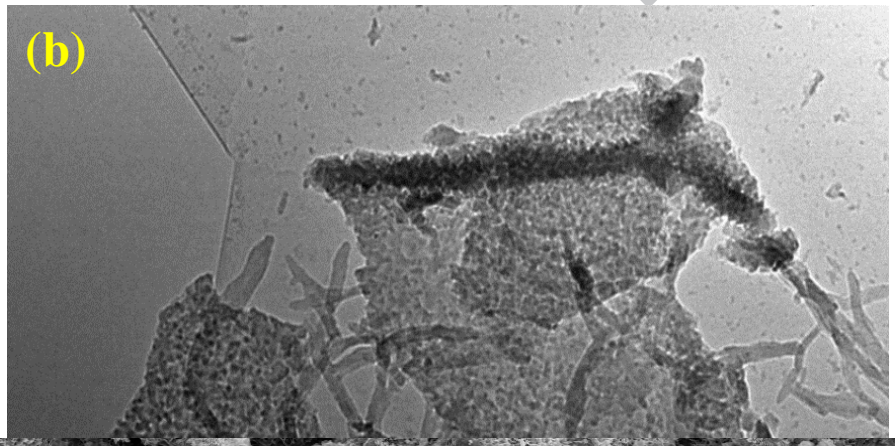

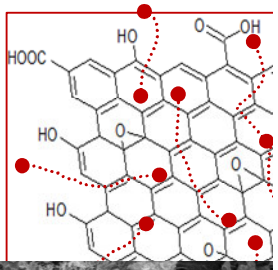

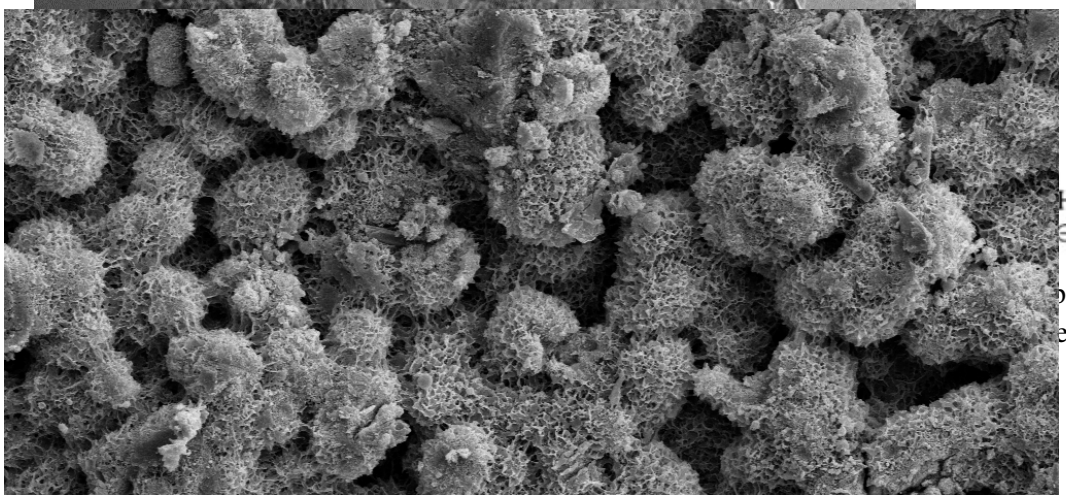

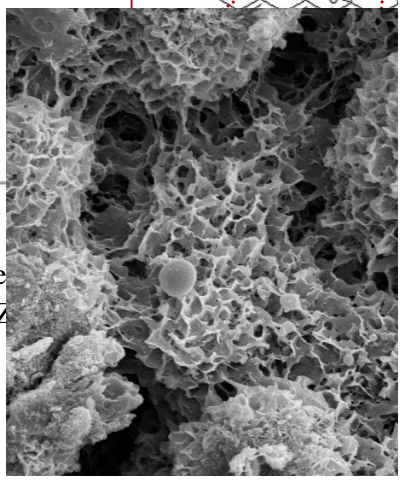

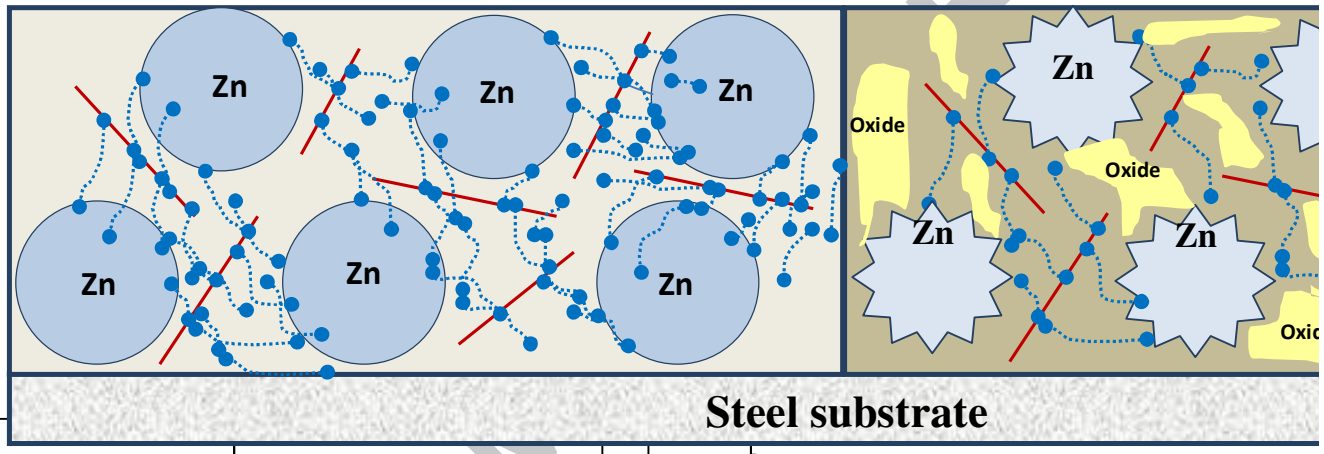

Figure 10- High magnification FE-SEM micrographs of the GO-PANI/ZRC sample after 1000 h salt spray te

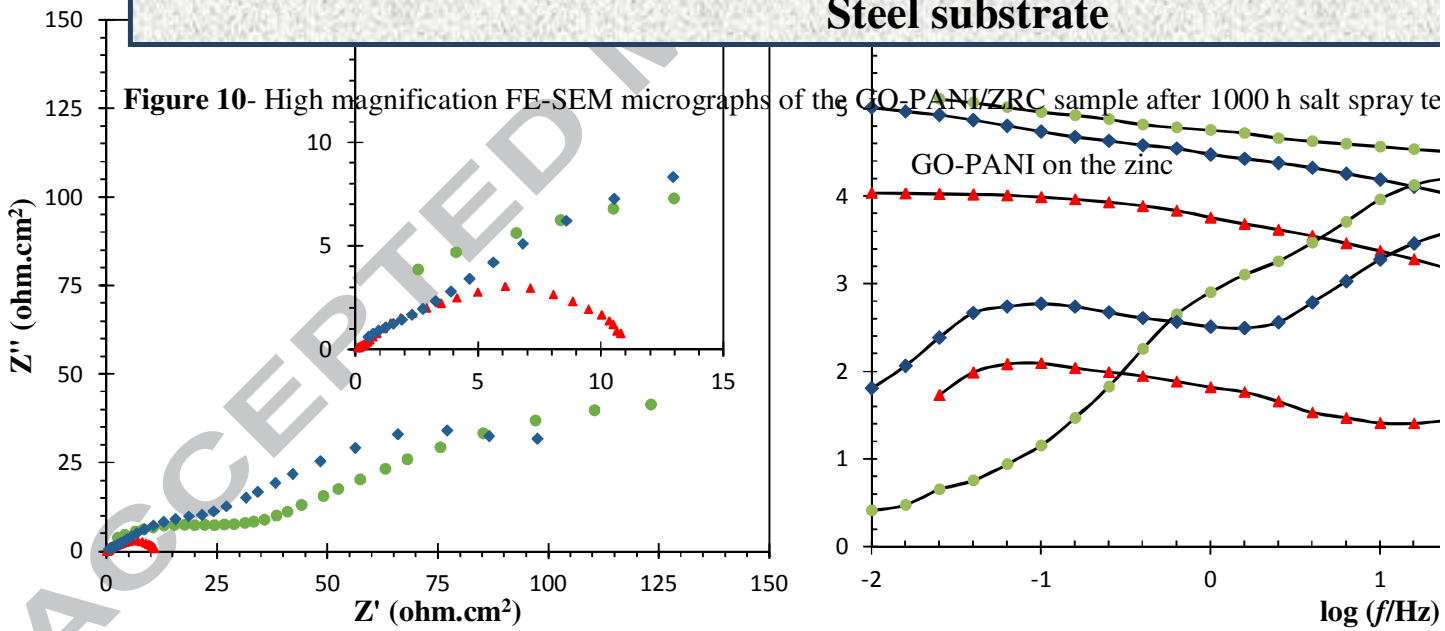

Figure 11- Nyquist and Bode diagrams of the ZRC sample after 10, 10 and 50 days immersion in 3.5 wt.% NaCl solution

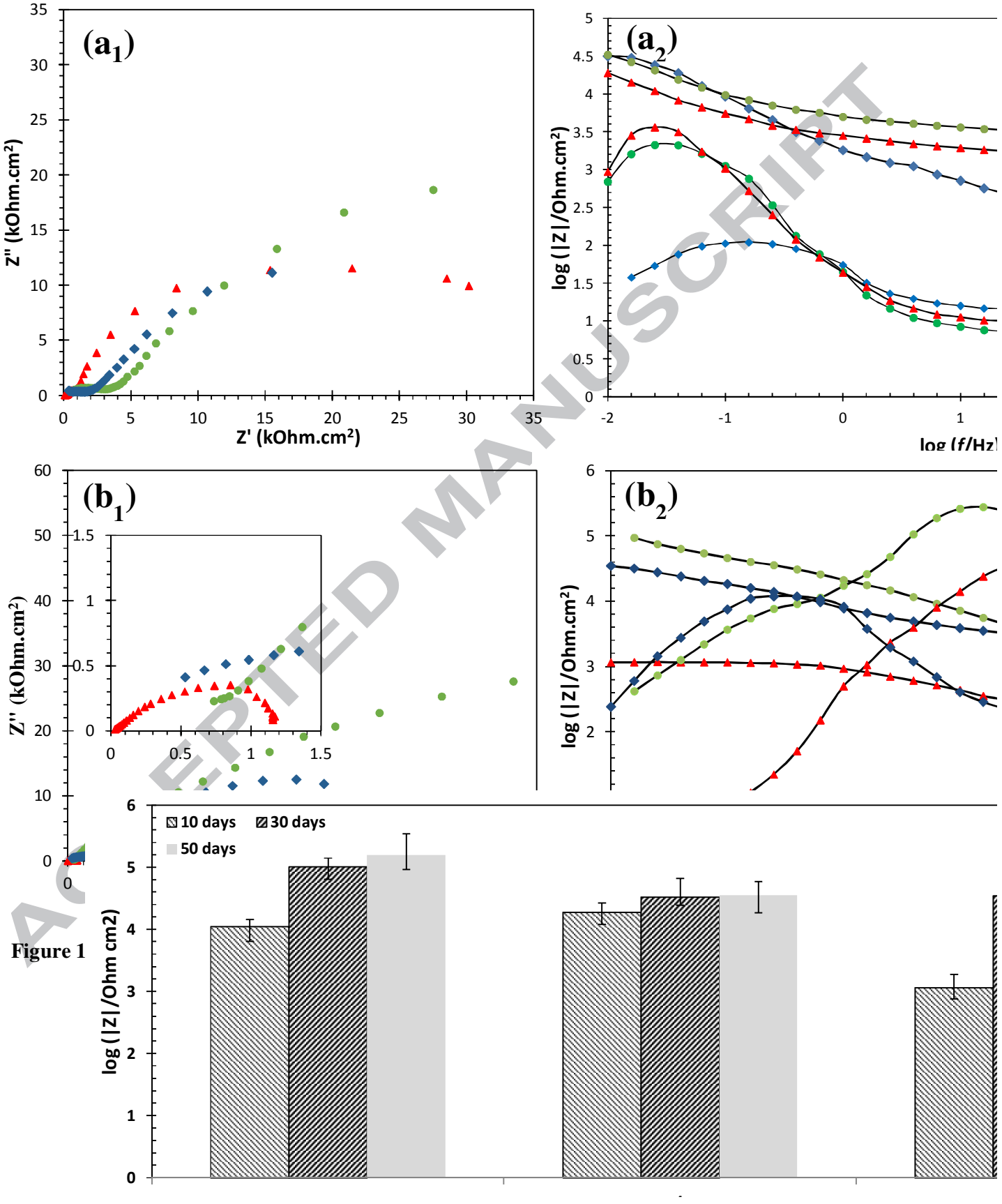

Figure 1

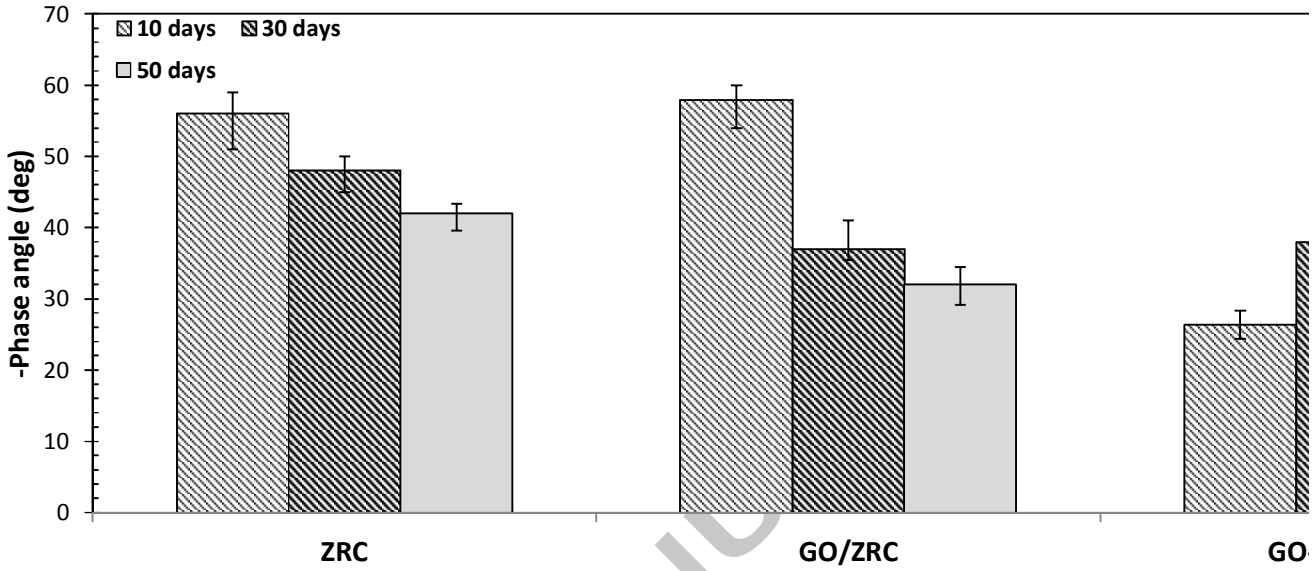

Figure 13. (a) The values of impedance at 10 mHz and (b) phase angle at 10 kHz obtained from Bode di

immersion in 3.5 wt.% NaCl solution

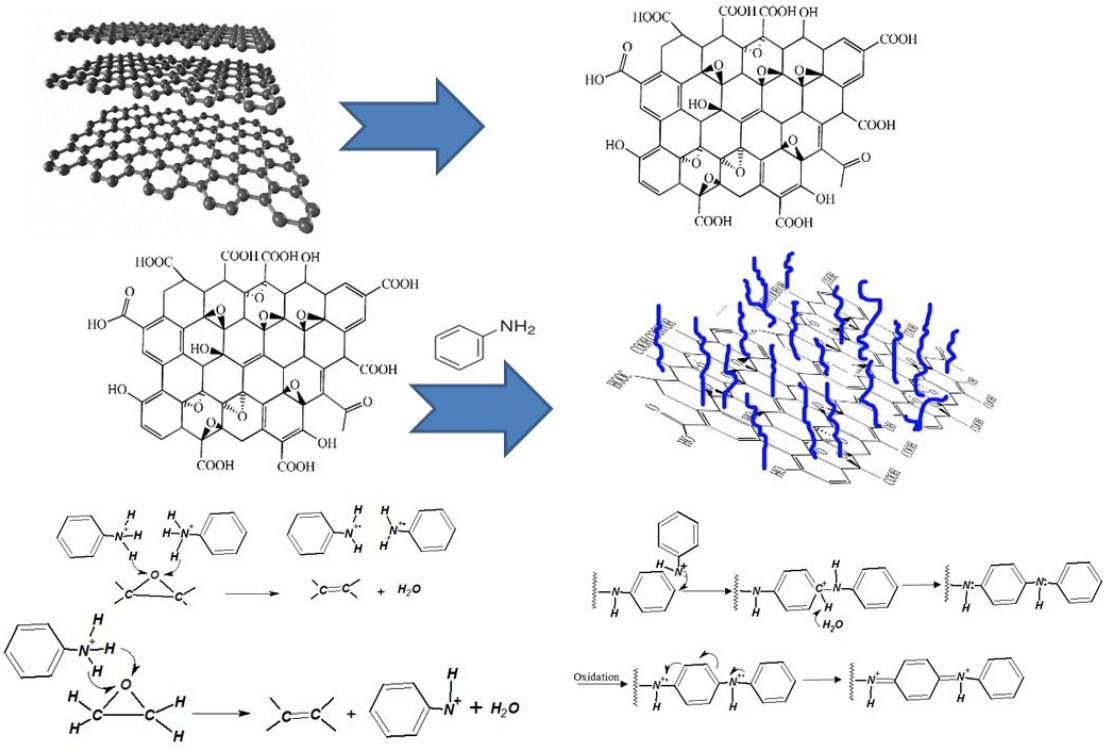

Table 1: EDS results before and after 30 days immersion of ZRC, GO/ZRC and GO-PANI/ZRC samples in 3.5 wt.% NaCl solution

Sample	ZRC		GO/ZRC		GO-PANI/ZRC	
	Before	*After*	*Before*	*After*	*Before*	*After*
Zn	45.2	38.2	47.5	32.8	48.2	43.3
O	16.3	25.9	15.7	20.3	16.4	18.1
C	32.2	30.9	31.4	33.2	28.3	31.7
N	6.3	2.4	5.4	13.0	7.1	6.9
Fe	0	2.6	0	0.7	0	0

- Modification of GO by polyaniline nanofibers enhanced its electrical conductivity
- Barrier properties of zinc rich paint remarkably increased after addition of GO-PANI
- GO-PANI enhanced the electrical contact between zinc particles and steel substrate
- The zinc rich sacrificial behavior noticeably enhanced after addition of GO-PANI